International Journal of Heat and Technology
Vol. 36, No. 1, March, 2018, pp. 1-10
Journal homepage: http://iieta.org/Journals/IJHT

The study of three dimensional radiative mhd casson nanofluid over an exponential porous stretching sheet with heat source under convective boundary conditions

Prathi V. Kumar[1], Shaik M. Ibrahim[1*], Giulio Lorenzini[2]

[1] Department of Mathematics, GITAM Deemed to be University, Visakhapatnam, Andhra Pradesh 530045, India
[2] Department of Engineering and Architecture, University of Parma, Parco Area delle Scienze 181/A Parma 43124, Italy

Corresponding Author Email: ibrahimsvu@gmail.com

https://doi.org/10.18280/ijht.360101

Received: 10 December 2017
Accepted: 7 March 2018

Keywords:
three dimensional flow, casson fluid, exponentially stretching sheet, radiation, HAM.

ABSTRACT

The aspire of this study is to analyse the magnetohydrodynamic (MHD) three dimensional flow of nanofluid induced by an exponentially stretching sheet in the presence of radiation and heat source. Casson fluid model is espoused in this discussion. The repercussion of porous matrix on the Casson nanofluid is also considered. Analysis is carried out when the surface shows convective condition. Brownian motion and thermophoresis effects are considered. Governing equations are evolved and converted into ordinary differential equations using similarity transformations. We adopted homotopy analysis method (HAM) to pick up the solutions. Impact of various parameters is displayed through graphs and tables and discussed in detail. Dual solutions are established by taking Casson and Newtonian fluids. A comparison is made and the correspondence between the acquired and previous results reveals that they are in good correlation.

1. INTRODUCTION

The low thermal conductivity of conventional heat transfer fluids like water, engine oil, glycol, etc, made them incompetent to attain the modern cooling requirements. Nanofluids (homogeneous mixture of base fluid and nanoparticles) which carry high thermal conductivity are contributed as nonpareil coolants in various fields such as nuclear reactors, heat exchangers, micro-channel heat sinks, polymer extrusion, etc. The term 'nanofluid' was first described by Choi [1]. Prabhat et al. [2] studied the aberrant increase of thermal conductivity and viscosity in nanofluids. Khan and Pop [3] led to the study of nanofluid flow over a stretching sheet. Hady et al. [4] reported the radiation effect on nanofluid flow over a nonlinear stretching sheet. Rida et al. [5] made an analytical study on MHD nanofluid over a stretching sheet through a porous medium under thermal radiation and heat generation. Some recent studies concerning the flow of nanofluid fluid can be found in [6-9].

Three dimensional flow of non-Newtonian fluid plays a vital role in the fields like food processing, performance of lubricants, polymer processing, etc. Wang [10] induced the problem of three dimensional flow over a stretching surface. Ariel [11] obtained an approximate solution to the three dimensional flow past a stretching sheet. Liu et al. [12] analysed the boundary layer flow and heat transfer behaviour of three dimensional fluid flow over an exponentially stretching sheet. The above discussion can be found in Hayat et al. [13], Nadeem et al. [14], Jayachandra babu and Sandeep [15], Ahmed et al. [16] and soon.

Many researchers have allured the concept of Casson fluid [17] as they have gigantic applications in the fields like polymer processing, biomechanics, drilling operations, metallurgy, etc. Casson fluid constitutive equation delineate a nonlinear relationship among stress and rate of strain and has been observed to be perfectly admissible to silicon suspensions, suspensions of bentonite in water, and lithographic varnishes used for printing inks. Mukhopadhyay [18] reported that the Casson parameter depreciates the velocity field. Mustafa and Khan [19] discussed the magnetic field effect on Casson nanofluid over a nonlinearly stretching sheet. Ibrahim and Makinde [20] discussed the stagnation point flow of Casson nanofluid subject to slip and convective boundary conditions. Extensive literature on nanofluid flows can be found in [21-25].

Here we made an investigation to study the MHD three dimensional flow of Casson nanofluid over an exponentially stretching sheet. In the mathematical model convective condition, radiation and heat source effects are also considered. The obtained model was solved by HAM. It has been evinced that this technique is a magnificent approach in dealing with various problems [26-30].

2. MATHEMATICAL FORMULATION

Three dimensional steady incompressible MHD flow of Casson nanofluid in a porous medium over an exponentially stretching sheet with convective boundary condition under radiation and heat source is considered. The fluid is electrically conducting under the impact of uniform magnetic field B_o which is applied along the Z-direction. Induced magnetic field is not taken into account due to small Reynolds number. Thermophoresis and Brownian motion effects are considered. Physical model of the flow problem is given in Figure 1.

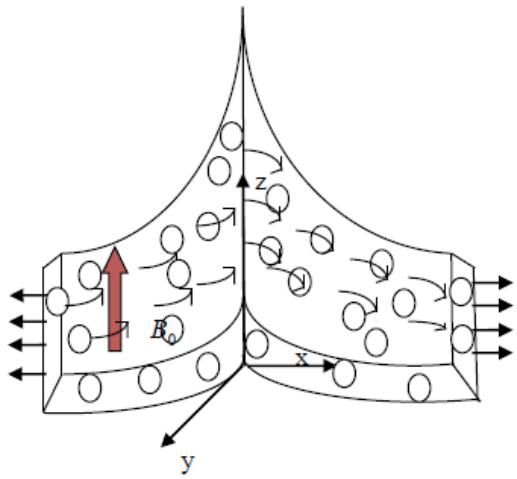

Figure 1. Physical model

The rheological equation of state for an isotropic and incompressible flow of Casson fluid is

$$\tau_{ij}=\begin{cases}2\left(\mu_B+\dfrac{p_y}{\sqrt{2\pi}}\right)e_{ij}, & \pi>\pi_c\\ 2\left(\mu_B+\dfrac{py}{\sqrt{2\pi_c}}\right)e_{ij}, & \pi_c>\pi\end{cases}$$

where μ_B is plastic dynamic viscosity of the non-Newtonian fluid, p_y is the yield stress of the fluid, π is the product of the component of deformation rate with itself, $\pi=e_{ij}e_{ij}$, e_{ij} is the $(i,j)^{th}$ component of the deformation rate and π_c is a critical value of this product, based on the non-Newtonian model. Under these assumptions, the equations governing the flow can be written as

$$\frac{\partial u}{\partial x}+\frac{\partial v}{\partial y}+\frac{\partial w}{\partial z}=0, \tag{1}$$

$$u\frac{\partial u}{\partial x}+v\frac{\partial u}{\partial y}+w\frac{\partial u}{\partial z}=\nu_f\left(1+\frac{1}{\beta}\right)\frac{\partial^2 u}{\partial z^2}-\frac{\sigma B_0^2 u}{\rho_f}-\frac{\nu_f u}{K^*}, \tag{2}$$

$$u\frac{\partial u}{\partial x}+v\frac{\partial u}{\partial y}+w\frac{\partial u}{\partial z}=\nu_f\left(1+\frac{1}{\beta}\right)\frac{\partial^2 v}{\partial z^2}-\frac{\sigma B_0^2 v}{\rho_f}-\frac{\nu_f v}{K^*}, \tag{3}$$

$$\begin{aligned}&u\frac{\partial T}{\partial x}+v\frac{\partial T}{\partial y}+w\frac{\partial T}{\partial z}=\alpha_f\frac{\partial^2 T}{\partial z^2}\\&+\tau\left[D_B\frac{\partial C}{\partial z}\frac{\partial T}{\partial z}+\frac{D_T}{T_\infty}\left(\frac{\partial T}{\partial z}\right)^2\right]-\frac{1}{(\rho c)_f}\left(\frac{\partial q_r}{\partial z}\right),\\&+\frac{Q_0}{(\rho c)_f}(T-T_\infty)\end{aligned} \tag{4}$$

$$u\frac{\partial C}{\partial x}+v\frac{\partial C}{\partial y}+w\frac{\partial C}{\partial z}=D_B\frac{\partial^2 C}{\partial z^2}+\frac{D_T}{T_\infty}\frac{\partial^2 T}{\partial z^2}. \tag{5}$$

The boundary conditions are

$$\begin{aligned}&u=U_w=U_0e^{\frac{x+y}{L}},\ v=V_w=V_0e^{\frac{x+y}{L}},\ w=0,\\&-k_f\left(\frac{\partial T}{\partial z}\right)=h_f\left(T_f-T\right),C=C_w\quad at\quad z=0,\\&u\to 0,\ v\to 0\quad T\to T_\infty,\quad C\to C_\infty\quad as\ \ z\to\infty.\end{aligned} \tag{6}$$

where $\alpha_f=\dfrac{k_f}{(\rho c)_f}$, $\tau=\dfrac{(\rho c)_p}{(\rho c)_f}$.

Using Rosseland approximation,

$$q_r=-\frac{4\sigma^*}{3k^*}\frac{\partial T^4}{\partial y}=\frac{16\sigma^* T_\infty^3}{3(\rho c)_f k^*}\frac{\partial^2 T}{\partial z^2}.$$

Now we induce the similarity transformations

$$\left.\begin{aligned}&u=U_0e^{\frac{x+y}{L}}f'(\xi),\ v=U_0e^{\frac{x+y}{L}}g'(\xi),\\&w=-\sqrt{\frac{\nu_f U_0}{2L}}e^{\frac{x+y}{2L}}\left[f(\xi)+\xi f'(\xi)+g(\xi)+\xi g'(\xi)\right]\\&\xi=z\sqrt{\frac{U_0}{2\nu_f L}}e^{\frac{x+y}{2L}},,\theta(\xi)=\frac{T-T_\infty}{T_f-T_\infty},\varphi(\xi)=\frac{C-C_\infty}{C_w-C_\infty},\end{aligned}\right\} \tag{7}$$

Here u, v and w satisfy the continuity equation. Eqs. (2) to (6) become

$$\left(1+\frac{1}{\beta}\right)f'''+(f+g)f''-2(f'+g')f'-(M+K)f'=0, \tag{8}$$

$$\left(1+\frac{1}{\beta}\right)g'''+(f+g)g''-2(f'+g')g'-(M+K)g'=0, \tag{9}$$

$$\left(1+\frac{4R}{3}\right)\theta''+\Pr\left[(f+g)\theta'+Nb\,\theta'\varphi'+Nt\,\theta'^2+Q\theta\right]=0, \tag{10}$$

$$\varphi''+Sc(f+g)\varphi'+\frac{Nt}{Nb}\theta'''=0. \tag{11}$$

The boundary conditions are

$$\begin{aligned}&f(0)=0,g(0)=0,f'(0)=1,g'(0)=\delta,\\&\theta'(0)=-B_i\left(1-\theta(0)\right),\varphi(0)=1,\\&f'(\infty)\to 0,g'(\infty)\to 0,\theta(\infty)\to 0,\varphi(\infty)\to 0.\end{aligned} \tag{12}$$

where $M=\dfrac{2\sigma B_0^2 L}{\rho_f U_w}$, $K=\dfrac{2\nu_f L}{U_w K^*}$, $\delta=\dfrac{V_0}{U_0}$, $R=\dfrac{4\sigma^* T_\infty^3}{k^* k}$,

$\Pr=\dfrac{\nu_f}{\alpha_f}$, $Nb=\dfrac{\tau D_B(C_w-C_\infty)}{\nu_f}$, $Nt=\dfrac{\tau D_B(T_f-T_\infty)}{T_\infty\nu_f}$,

$Q=\dfrac{2Q_0L}{U_w(\rho c)_f}$, $B_i=\dfrac{h_f}{k_f}\sqrt{\dfrac{2\nu_f L}{U_w}}$, $Sc=\dfrac{\nu_f}{D_B}$.

Non-dimensional skin friction coefficient in x and y directions C_{fx} and C_{fy}, local Nusselt number Nu_x and local Sherwood number Sh_x are

$$C_{fx}=\frac{2\tau_{wx}}{\rho_f U_w^2},\ C_{fy}=\frac{2\tau_{wy}}{\rho_f U_w^2}$$

where $\tau_{wy}=\mu_f\left(1+\frac{1}{\beta}\right)\left(\frac{\partial u}{\partial z}+\frac{\partial w}{\partial x}\right)_{z=0}$,

$\tau_{wy}=\mu_f\left(1+\frac{1}{\beta}\right)\left(\frac{\partial v}{\partial z}+\frac{\partial w}{\partial y}\right)_{z=0}$, $Nu_x=\frac{xq_w}{k_f\left(T_f-T_\infty\right)}$,

$q_w=-\left(k_f+\left(\frac{16\sigma^* T_\infty^3}{3k^*}\right)\left(\frac{\partial T}{\partial z}\right)\right)_{z=0}$ and $Sh_x=\frac{xq_m}{D_B\left(C_w-C_\infty\right)}$,

$q_m=-D_B\left(\frac{\partial C}{\partial z}\right)_{z=0}$.

Substituting q_w and q_m in the preceding equations, we get

$$\left(\frac{\mathrm{Re}}{2}\right)^{1/2}C_{fx}=\left(1+\frac{1}{\beta}\right)f''(0),\ \left(\frac{\mathrm{Re}}{2}\right)^{1/2}C_{fy}=\left(1+\frac{1}{\beta}\right)g''(0)$$

$$\left(\frac{\mathrm{Re}}{2}\right)^{-1/2}\frac{L}{x}Nu_x=-\left(1+\frac{4}{3}R\right)\theta'(0)$$

and $\left(\frac{\mathrm{Re}}{2}\right)^{-1/2}\frac{L}{x}Sh_x=-\varphi'(0)$

where $\mathrm{Re}=\frac{U_w L}{v_f}$ is the local Reynolds number.

3. HAM

To capture the homotopic solutions of Eqs. (8) to (12), we pick up the initial guesses and linear operators as follows:

$$\begin{aligned}
f_0(\xi)&=\left(1-e^{-\xi}\right),\\
g_0(\xi)&=\delta\left(1-e^{-\xi}\right)\\
\theta_0(\xi)&=\left(\frac{Bi\,e^{-\xi}}{1+Bi}\right),\\
\varphi_0(\xi)&=e^{-\xi}.
\end{aligned}\tag{13}$$

$$\begin{aligned}
L_1(f)&=f'''-f',\\
L_2(f)&=g'''-g'\\
L_3(\theta)&=\theta''-\theta,\\
L_4(\varphi)&=\varphi''-\varphi.
\end{aligned}\tag{14}$$

with the following properties

$$\begin{aligned}
L_1\left(C_1+C_2e^{\xi}+C_3e^{-\xi}\right)&=0,\\
L_2\left(C_4+C_5e^{\xi}+C_6e^{-\xi}\right)&=0,\\
L_3\left(C_7e^{\xi}+C_8e^{-\xi}\right)&=0,\\
L_4\left(C_9e^{\xi}+C_{10}e^{-\xi}\right)&=0,
\end{aligned}$$

where C_i(i=1 to 10) are the arbitrary constants.

We construct the zeroth-order deformation equations

$$(1-p)L_1\left(f(\xi;p)-f_0(\xi)\right)=p\hbar_1 N_1\left[f(\xi;p),g(\xi;p)\right],\tag{15}$$

$$(1-p)L_2\left(g(\xi;p)-g_0(\xi)\right)=p\hbar_2 N_2\left[f(\xi;p),g(\xi;p)\right],\tag{16}$$

$$(1-p)L_3\left(\theta(\xi;p)-\theta_0(\xi)\right)=p\hbar_3 N_3\begin{bmatrix}f(\xi;p),g(\xi;p),\\ \theta(\xi;p),\varphi(\xi;p)\end{bmatrix},\tag{17}$$

$$(1-p)L_4\left(\varphi(\xi;p)-\varphi_0(\xi)\right)=p\hbar_4 N_4\begin{bmatrix}f(\xi;p),g(\xi;p),\\ \theta(\xi;p),\varphi(\xi;p)\end{bmatrix},\tag{18}$$

subject to the boundary conditions

$$\begin{aligned}
&f(0;p)=0, && f'(0;p)=1, && f'(\infty;p)=0,\\
&g(0;p)=0, && g'(0;p)=\delta, && g'(\infty;p)=0,\\
&\theta'(0;p)=-B_i\left[1-\theta(0;p)\right], && && \theta(\infty;p)=0,\\
&\varphi(0;p)=1, && && \varphi(\infty;p)=0,
\end{aligned}\tag{19}$$

$$\begin{aligned}
N_1\left[f(\xi;p),g(\xi;p)\right]&=\left(1+\frac{1}{\beta}\right)\frac{\partial^3 f(\xi;p)}{\partial\xi^3}\\
&+\left(f(\xi;p)+g(\xi;p)\right)\frac{\partial^2 f(\xi;p)}{\partial\xi^2}\\
&-2\left(\frac{\partial f(\xi;p)}{\partial\xi}+\frac{\partial g(\xi;p)}{\partial\xi}\right)\frac{\partial f(\xi;p)}{\partial\xi}-(M+K)\frac{\partial f(\xi;p)}{\partial\xi},
\end{aligned}\tag{20}$$

$$\begin{aligned}
N_2\left[f(\xi;p),g(\xi;p)\right]&=\left(1+\frac{1}{\beta}\right)\frac{\partial^3 g(\xi;p)}{\partial\xi^3}\\
&+\left(f(\xi;p)+g(\xi;p)\right)\frac{\partial^2 g(\xi;p)}{\partial\xi^2}\\
&-2\left(\frac{\partial f(\xi;p)}{\partial\xi}+\frac{\partial g(\xi;p)}{\partial\xi}\right)\frac{\partial g(\xi;p)}{\partial\xi}-(M+K)\frac{\partial g(\xi;p)}{\partial\xi},
\end{aligned}\tag{21}$$

$$\begin{aligned}
N_3\left[f(\xi;p),g(\xi;p)\theta(\xi;p),\varphi(\xi;p)\right]&=\left(1+\frac{4}{3}R\right)\frac{\partial^2\theta(\xi;p)}{\partial\xi^2}\\
&+\mathrm{Pr}\left(\left(f(\xi;p)+g(\xi;p)\right)\frac{\partial\theta(\xi;p)}{\partial\xi}\right)\\
&+\mathrm{Pr}\begin{pmatrix}Nb\frac{\partial\theta(\xi;p)}{\partial\xi}\frac{\partial\varphi(\xi;p)}{\partial\xi}+Nt\left(\frac{\partial\theta(\xi;p)}{\partial\xi}\right)^2,\\ +Q\theta(\xi;p)\end{pmatrix}
\end{aligned}\tag{22}$$

$$N_3\left[f(\xi;p),g(\xi;p),\theta(\xi;p),\varphi(\xi;p)\right]=\frac{\partial^2\varphi(\xi;p)}{\partial\xi^2}$$
$$+Sc\left(f(\xi;p)+g(\xi;p)\right)\frac{\partial\varphi(\xi;p)}{\partial\xi}+\left(\frac{Nt}{Nb}\right)\frac{\partial^2\theta(\xi;p)}{\partial\xi^2}, \tag{23}$$

When $p=0$ and $p=1$, we obtain

$$\begin{aligned} f(\xi;0)&=f_0(\xi) & f(\xi;1)&=f(\xi),\\ g(\xi;0)&=g_0(\xi) & g(\xi;1)&=g(\xi),\\ \theta(\xi;0)&=\theta_0(\xi) & \theta(\xi;1)&=\theta(\xi),\\ \varphi(\xi;0)&=\varphi_0(\xi) & \varphi(\xi;1)&=\varphi(\xi). \end{aligned} \tag{24}$$

Thus, as p increases from 0 to 1 then $f(\xi;p)$, $g(\xi;p)$, $\theta(\xi;p)$ and $\varphi(\xi;p)$ vary from initial approximations to the exact solutions of the original nonlinear differential equations.

Now, expanding $f(\xi;p)$, $g(\xi;p)$, $\theta(\xi;p)$ and $\varphi(\xi;p)$ in Taylor's series w.r.to p, we have

$$f(\xi;p)=f_0(\xi)+\sum_{m=1}^{\infty}f_m(\xi)\,p^m, \tag{25}$$

$$g(\xi;p)=g_0(\xi)+\sum_{m=1}^{\infty}g_m(\xi)\,p^m, \tag{26}$$

$$\theta(\xi;p)=\theta_0(\xi)+\sum_{m=1}^{\infty}\theta_m(\xi)\,p^m, \tag{27}$$

$$\varphi(\xi;p)=\varphi_0(\xi)+\sum_{m=1}^{\infty}\varphi_m(\xi)\,p^m, \tag{28}$$

where

$$\begin{aligned} f_m(\xi)&=\frac{1}{m!}\frac{\partial^m f(\xi;p)}{\partial p^m}\bigg|_{p=0},\\ g_m(\xi)&=\frac{1}{m!}\frac{\partial^m g(\xi;p)}{\partial p^m}\bigg|_{p=0},\\ \theta_m(\xi)&=\frac{1}{m!}\frac{\partial^m \theta(\xi;p)}{\partial p^m}\bigg|_{p=0},\\ \varphi_m(\xi)&=\frac{1}{m!}\frac{\partial^m \varphi(\xi;p)}{\partial p^m}\bigg|_{p=0}. \end{aligned} \tag{29}$$

If the initial approximations, auxiliary linear operators and non-zero auxiliary parameters are chosen in such a way that the series (25) to (28) are convergent at $p=1$, then

$$f(\eta)=f_0(\xi)+\sum_{m=1}^{\infty}f_m(\xi), \tag{30}$$

$$g(\eta)=g_0(\xi)+\sum_{m=1}^{\infty}g_m(\xi), \tag{31}$$

$$\theta(\xi)=\theta_0(\xi)+\sum_{m=1}^{\infty}\theta_m(\xi), \tag{32}$$

$$\varphi(\xi)=\varphi_0(\xi)+\sum_{m=1}^{\infty}\varphi_m(\xi). \tag{33}$$

Differentiating Eqs. (15) to (19) m times w.r.to p, setting $p=0$ and finally dividing with $m!$, we get the mth-order deformation equations as follows:

$$L_1\left(f_m(\xi)-\chi_m\,f_{m-1}(\xi)\right)=\hbar_1\,R_m^f(\xi), \tag{34}$$

$$L_2\left(g_m(\xi)-\chi_m\,g_{m-1}(\xi)\right)=\hbar_2\,R_m^g(\xi), \tag{35}$$

$$L_3\left(\theta_m(\xi)-\chi_m\,\theta_{m-1}(\xi)\right)=\hbar_3\,R_m^\theta(\xi), \tag{36}$$

$$L_4\left(\varphi_m(\xi)-\chi_m\,\varphi_{m-1}(\xi)\right)=\hbar_4\,R_m^\varphi(\xi), \tag{37}$$

with the following boundary conditions

$$\begin{aligned} &f_m(0)=0, \quad f_m'(0)=0, \quad f_m'(\infty)=0,\\ &g_m(0)=0, \quad g_m'(0)=0, \quad g_m'(\infty)=0,\\ &\theta_m'(0)=0, \qquad\qquad \theta_m(\infty)=0,\\ &\varphi_m(0)=0, \qquad\qquad \varphi_m(\infty)=0, \end{aligned} \tag{38}$$

where

$$\begin{aligned} R_m^f(\xi)&=\left(1+\frac{1}{\beta}\right)f_{m-1}'''+\sum_{i=0}^{m-1}\left(f_{m-1-i}+g_{m-1-i}\right)f_i''\\ &-2*\sum_{i=0}^{m-1}\left(f_{m-1-i}'+g_{m-1-i}'\right)f_i'-(M+K)\,f_{m-1}', \end{aligned} \tag{39}$$

$$\begin{aligned} R_m^g(\xi)&=\left(1+\frac{1}{\beta}\right)g_{m-1}'''+\sum_{i=0}^{m-1}\left(f_{m-1-i}+g_{m-1-i}\right)g_i''\\ &-2*\sum_{i=0}^{m-1}\left(f_{m-1-i}'+g_{m-1-i}'\right)g_i'-(M+K)\,g_{m-1}', \end{aligned} \tag{40}$$

$$R_m^\theta(\xi)=\left(1+\frac{4R}{3}\right)\theta_{m-1}''+Pr\begin{pmatrix}\sum_{i=0}^{m-1}\left(f_{m-1-i}+g_{m-1-i}\right)\theta_i'\\ +Nb\sum_{i=0}^{m-1}\theta_{m-1-i}'\,\varphi_i'\\ +Nt\sum_{i=0}^{m-1}\theta_{m-1-i}'\,\theta_i'\\ +Q\,\theta_{m-1}\end{pmatrix}, \tag{41}$$

$$\begin{aligned} R_m^\varphi(\xi)&=\varphi_{m-1}''+Sc\left(\sum_{i=0}^{m-1}\left(f_{m-1-i}+g_{m-1-i}\right)\varphi_i'\right)\\ &+\left(\frac{Nt}{Nb}\right)\theta_{m-1}'', \end{aligned} \tag{42}$$

$$\chi_m=\begin{cases}0, & m\le 1,\\ 1, & m>1.\end{cases} \tag{43}$$

If we let $f_m^*(\xi)$, $g_m^*(\xi)$, $\theta_m^*(\xi)$ and $\varphi_m^*(\xi)$ as the special solutions of mth order deformation equations, then the general solution is given by

$$\begin{aligned} f_m(\xi) &= f_m^*(\xi) + C_1 + C_2 e^{\xi} + C_3 e^{-\xi}, \\ g_m(\xi) &= g_m^*(\xi) + C_4 + C_5 e^{\xi} + C_6 e^{-\xi}, \\ \theta_m(\xi) &= \theta_m^*(\xi) + C_7 e^{\xi} + C_8 e^{-\xi}, \\ \varphi_m(\xi) &= \varphi_m^*(\xi) + C_9 e^{\xi} + C_{10} e^{-\xi}, \end{aligned} \tag{44}$$

where the integral constants $C_i\,(i = 1\ to\ 10)$ are determined using the boundary conditions.

4. CONVERGENCE OF HAM

The convergence and rate of approximation of the procured results strongly rely on on the auxiliary parameters $\hbar_1, \hbar_2, \hbar_3$ and $\hbar_4$. To acquire the relevant values for these parameters, $\hbar$-curves are portrayed in Figure 2. From this diagrammatic representation, it is scrutinized that the plausible region of the parameters is about $[-0.94, 0.0]$. For $\hbar_1 = \hbar_2 = \hbar_3 = \hbar_4 = -0.52$, the series solutions are convergent in the whole region of ξ. Table 1 displays the convergence of the method.

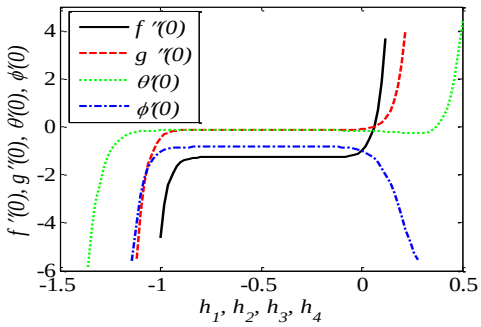

Figure 2. $\hbar$-curves for $f''(0), g''(0), \theta'(0)$ and $\varphi'(0)$ at 15th order approximations

Table 1. Convergence of HAM solution for different orders of approximations when

Order	$-f''(0)$	$-g''(0)$	$-\theta'(0)$	$-\varphi''(0)$
5	1.903651	0.190365	0.169773	0.834825
10	1.903677	0.190368	0.167740	0.844751
15	1.903677	0.190368	0.167613	0.844049
20	1.903677	0.190368	0.167591	0.844287
25	1.903677	0.190368	0.167588	0.844253
30	1.903677	0.190368	0.167588	0.844256
35	1.903677	0.190368	0.167588	0.844256
40	1.903677	0.190368	0.167588	0.844256

5. RESULTS AND DISCUSSION

In this, we panoply some results which bring acumen about the problem. For these computations, we consider the following values all over the study except refurbished values as delivered in the tables and graphs. The results are taken for Newtonian and Casson fluids.

$M = 0.5, \delta = K = R = 0.1, \Pr = 2.0, Nb = Nt = 0.2,$
$Q = 0.1, B_i = 0.2, Sc = 2.0.$

Lorentz force impinges its resistance on fluid motion as a result axial and transverse velocities get decelerated with Hartmann parameter M. This is shown in Figures 3 and 4. Figures 5 and 6 depict that the velocities in both directions diminish as the porous parameter K enhances. This is due to the Darcy resistance provided by the porous medium. Figures 7 and 8 illustrate the impact of ratio parameter δ on both the velocities. Amplification in δ implies an immensive stretching rate in the y-direction and thus the velocity in the y-direction raises whereas the velocity in the x-direction decelerates correspondingly. An increase in Prandtl number $\Pr$ constitutes devaluation in the temperature field. Physically larger Prandtl number has feeble thermal diffusivity due to which lower temperature is observed in Figure 9. It is noticed from Figure 10 that a raise in radiation parameter R has the capability to enhance the thermal boundary layer and consequently the fluid temperature rises.

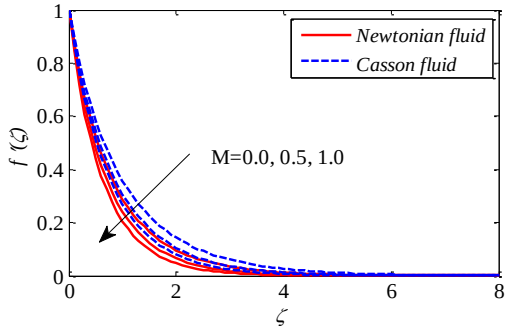

Figure 3. Effect of M on $f'(\xi)$

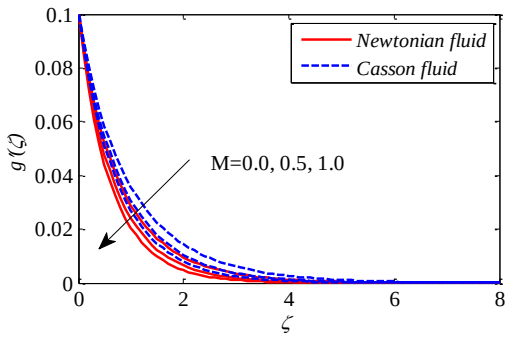

Figure 4. Effect of M on $g'(\xi)$

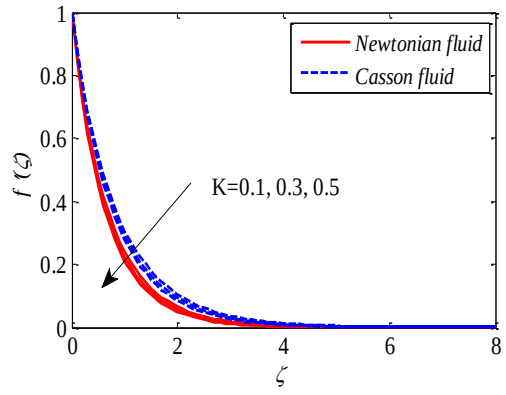

Figure 5. Effect of K on $f'(\xi)$

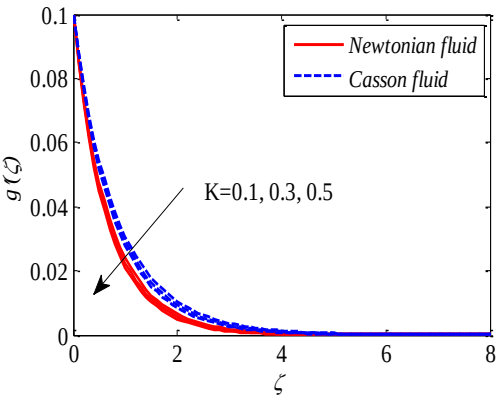

Figure 6. Effect of K on $g'(\xi)$

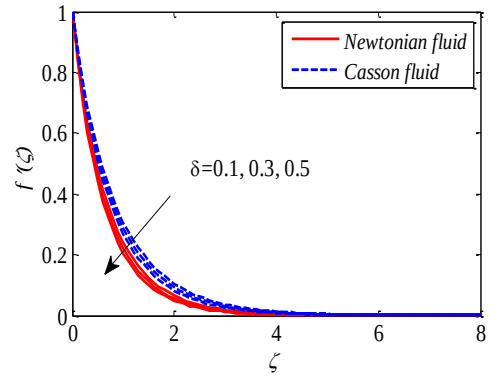

Figure 7. Effect of δ on $f'(\xi)$

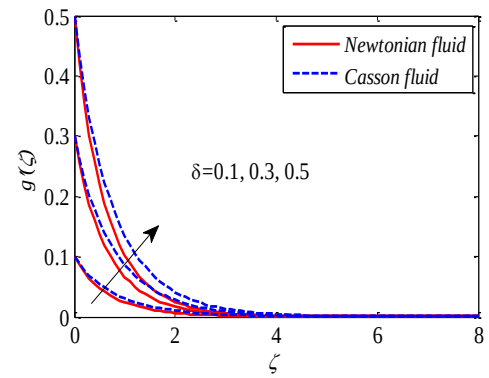

Figure 8. Effect of δ on $g'(\xi)$

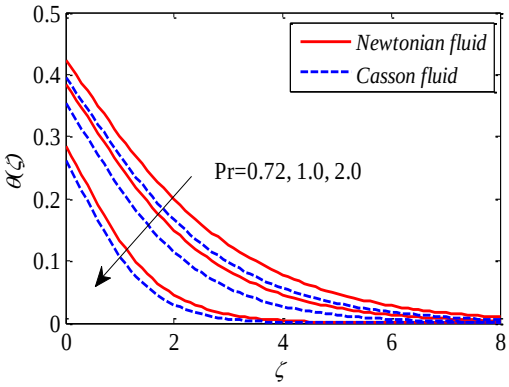

Figure 9. Effect of Pr on $\theta(\xi)$

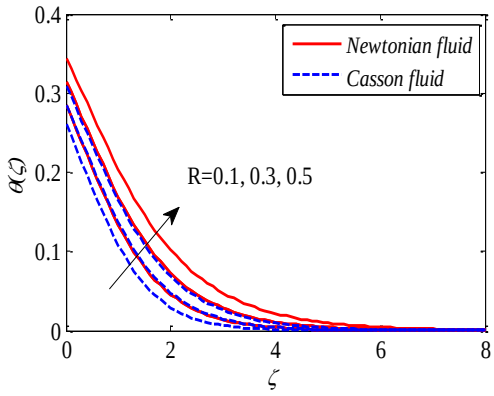

Figure 10. Effect of R on $\theta(\xi)$

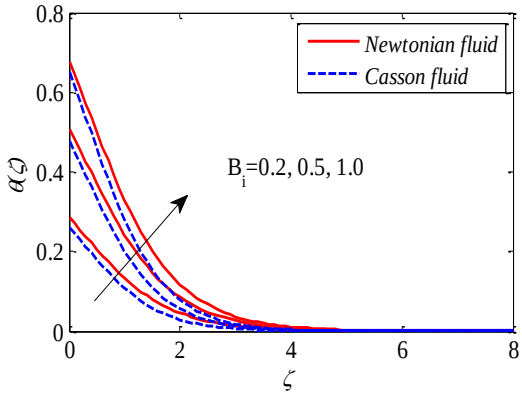

Figure 11. Effect of B_i on $\theta(\xi)$

Figure 11 illustrate that enhancing values of Biot number B_i uplift the temperature. Physically an increase in Biot number causes an enhancement in the heat transfer coefficient which up lift the thermal energy to the fluid and thus temperature increases. In the existence of heat source parameter Q in the fluid, thermal energy is released and as a repercussion, temperature increases. This is shown in Figure 12. The influence of Brownian motion and thermophoresis parameters Nb and Nt on temperature field is given in Figurs 13 and 14. These parameters are arrived due to the existence of nanoparticles which enhance the thermal conductivity of the fluid as a result temperature increases with Nb and Nt. It is observed that the impact of these parameters is significantly high in Newtonian fluid while compared with the Casson fluid. The effect of Brownian motion and thermophoresis parameters Nb and Nt on concentration field is given in Figurs 15 and 16. Enhancing values of Nt shows stronger thermophoretic force which deviates the nanoparticles from the hot sheet to the quiescent fluid thereby increasing the nanoparticle volume fraction boundary layer. Hence concentration enhances with Nt. But we pointed out an opposite phenomena in the concentration profiles with an increase in the Brownian motion parameter. Figure 17 indicates the influence of Schmidt number Sc on concentration profiles. It is observed that concentration depreciates with Sc. It is due to the fact that increasing values of Sc results a weaker Brownian coefficient. From the Figurs 18 and 19, it is observed that the skin friction coefficients are decelerating with the increasing values of magnetic parameter M and porous parameter K. Local Nusselt number increases with Biot number B_i and

radiation parameter R. This is shown in Figure 20. Sherwood number is enhancing with the increase of Schmidt number Sc and diminishing with thermophoresis parameter Nt. This is given in Figure. 21.

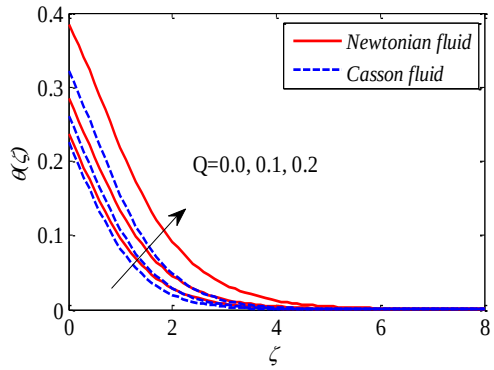

Figure 12. Effect of Q on $\theta(\xi)$

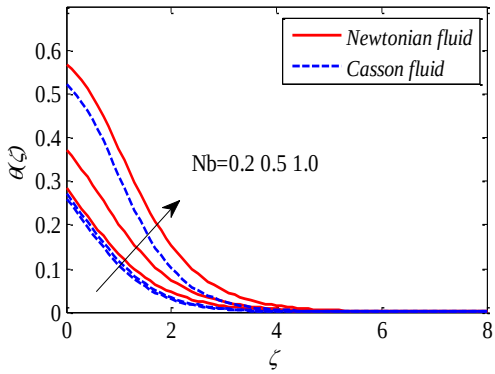

Figure 13. Effect of Nb on $\theta(\xi)$

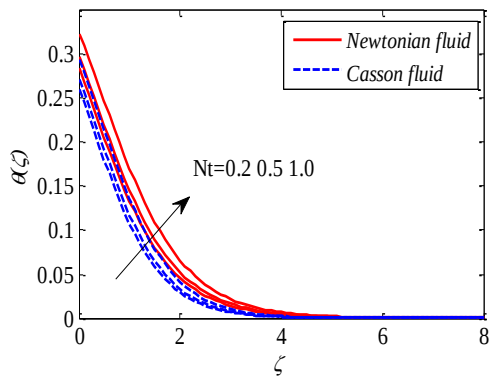

Figure 14. Effect of Nt on $\theta(\xi)$

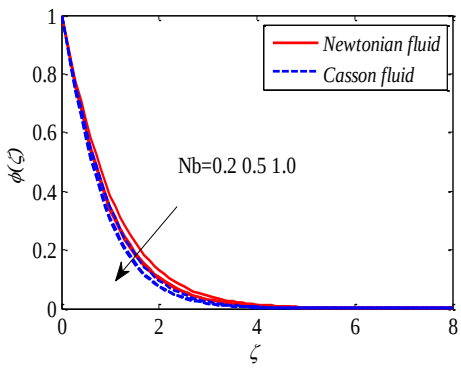

Figure 15. Effect of Nb on $\varphi(\xi)$

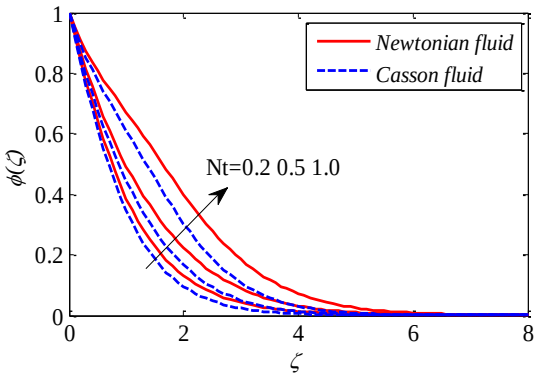

Figure 16. Effect of Nt on $\varphi(\xi)$

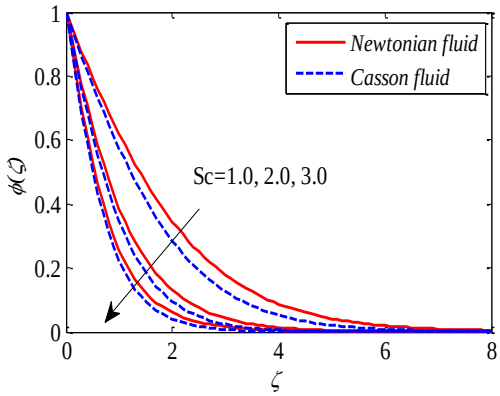

Figure 17. Effect of Sc on $\varphi(\xi)$

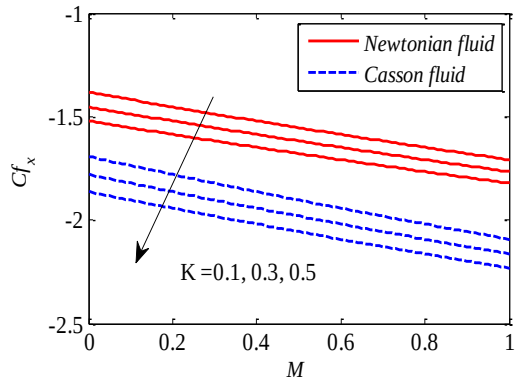

Figure 18. Effect of M and K on C_{fx}

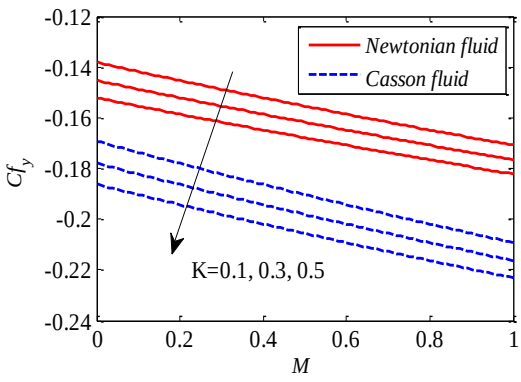

Figure 19. Effect of M and K on C_{fy}

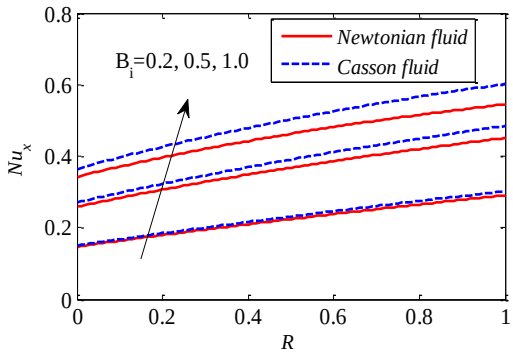

Figure 20. Effect of B_i and R on Nu_x

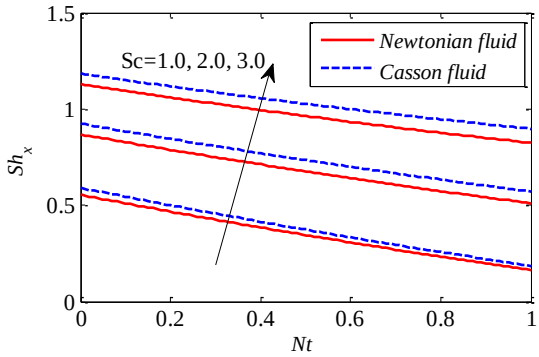

Figure 21. Effect of Nt and Sc on Sh_x

To endorse the veracity of the present analysis, the obtained results of $-f''(0)$ and have been compared with that of Liu et al. [12] solutions for the limiting case and.

Table 2. Comparison of and

	Liu et al. [12]		HAM	
0.0	1.28180856	0	1.281826	0
0.5	1.56988846	0.78494423	1.569889	0.784944
1.0	1.81275105	1.81275105	1.812752	1.812752

6. CONCLUSIONS

In this article a detailed scrutiny is accomplished to study the three dimensional steady incompressible MHD flow of Casson nanofluid over an exponentially stretching sheet with convective boundary condition under radiation and heat source. Brownian motion and thermophoresis effects are considered in the flow region. HAM is used to solve the nonlinear ordinary differential equations. Following are the major findings of the analysis:

- Increase in reduces the axial velocity where as reverse trend is observed in transverse velocity.
- The impact of and is significantly high in Newtonian fluid while compared with the Casson fluid.
- Schmidt number has propensity to decelerate the concentration field.
- It is seen that an increase in radiation parameter causes more impact on temperature field of the Newtonian fluid when compared with the Casson fluid.

REFERENCES

[1] Choi SUS. (1995). Enhancing thermal conductivity of fluids with nanoparticles. Proceedings of the 1995 ASME International Mechanical Engineering Congress and Exposition, San Francisco, 99-105.

[2] Prabhat N, Buongiorno J, Hu LW. (2012). Convective heat transfer enhancement in nanofluids: Real anomaly or analysis artifact. Journal of Nanofluids 1(1): 55-62. https://doi.org/ 10.1166/jon.2012.1003

[3] Khan WA, Pop I. (2010). Boundary layer flow of a nanofluid past a stretching sheet. Int. J. Heat Mass Transfer 53(11-12): 2477-2483. https://doi.org/ 10.1016/j.ijheatmasstransfer.2010.01.032

[4] Hady FM, Ibrahim FS, Abdel-Gaied SM, Eid MR. (2012). Radiation effect on viscous flow of a nanofluid and heat transfer over a nonlinearly stretching sheet. Nanoscale Research Letters 7: 229-242. https://doi.org/ 10.1186/1556-276X-7-229

[5] Rida SZ, Mohamed RA, Mubarak MS. (2016). MHD nanofluid flow over a stretching sheet through a porous medium with heat generation and thermal radiation. Journal of Nanofluids 5(1): 130-138. https://doi.org/ 10.1166/jon.2016.1187

[6] Mabood F, Khan WA, Ismail AIM. (2015). MHD boundary layer flow and heat transfer of nanofluids over a nonlinear stretching sheet: A numerical study. J. Magn. Magn. Mater 374: 569-576. https://doi.org/ 10.1016/j.jmmm.2014.09.013

[7] Haq RU, Nadeem S, Khan ZH, Sher Akbar N. (2015). Thermal radiation and slip effects on MHD stagnation point flow of nanofluid over a stretching sheet. Physica E: Low-dimensional system and Nanostructure 65: 17-23. https://doi.org/ 10.1016/j.physe.2014.07.013

[8] Raashidi MM, Vishnu Ganesh N, Abdul Hskeem AK, Ganga B. (2014). Buoyancy effect on MHD flow of nanofluid over a stretching sheet in the presence of thermal radiation. J. Mol. Liq. 198: 234-238. https://doi.org/ 10.1016/j.molliq.2014.06.037

[9] Nadeem N, Haq RU, Khan ZH. (2014). Numerical solution of non-Newtonian nanofluid over a stretching sheet. Applied Nanoscience 4(5): 625-631. https://doi.org/ 10.1007/s13204-013-0235-8

[10] Wang CY. (1984). The three-dimensional flow due to a stretching flat surface. Phys. Fluids 27: 1915-1917. https://doi.org/ 10.1063/1.864868

[11] Ariel PD. (2007). On computation of the three-dimensional flow past a stretching sheet. Appl. Math. Comput. 188(2): 1244-1250. https://doi.org/ 10.1016/j.amc.2006.10.083

[12] Liu IC, Wang HH, Peng YF. (2014). Flow and heat transfer for three dimensional flow over an exponentially stretching surface. Chem. Eng, Commun. 200(2): 253-268. https://doi.org/ 10.1080/00986445.012.703148

[13] Hayat T, Shehzad SA, Alsaedi A. (2014). MHD three-dimensional flow by an exponentially stretching surface with convective boundary condition. J. Aerosp. Eng. 27(4): 04014011. https://doi.org/ 10.1061/(ASCE)AS.1943-5525.0000360

[14] Nadeem S, Haq RU, Khan ZH. (2014). Heat transfer analysis of water-based nanofluid over an exponentially stretching sheet. Alexandria Engineering Journal 53: 219-224, 2014. https://doi.org/ 10.1016/j.aej.2013.11.003

[15] Jayachandra babu M, Sandeep N. (2016). Three-dimensional MHD slip flow of nanofluids over a slendering stretching sheet with thermophoresis and Brownian motion effects. Advanced Power Technology 27(5): 2039-2050. https://doi.org/ 10.1016/japt.2016.07.013
[16] Ahmed N, Kalita H, Barua D. (2012). An oscillatory three dimensional flow past an infinite vertical porous plate with soret and Dufour effects. International Journal of Heat and Technology 30(2): 9-18. https://doi.org/ 10.18280/ijht.300202
[17] Casson N. (1959). A flow equation for pigment oil suspensions of the printing ink type. Rheology of Disperse Systems: Proceedings of a Conference Organized by the British Society of Rheology., New York, pp. 84-104.
[18] Mukhopadhyay S. (2013). Casson fluid flow and heat transfer over a nonlinear surface. Chinese. Phy. B. 22(7): 074701. https://doi.org/ 10.1088/1674-1056/22/7/074701
[19] Mustafa M, Khan JA. (2015). Model for flow of Casson nanofluid past a non-linearly stretching sheet considering magnetic effects. AIP Advances 5: 07748. https://doi.org/ 10.1063/1.4927449
[20] Ibrahim W, Makinde OD. (2016). Magnetohydrodynamic stagnation point flow and heat transfer of Casson nanofluid past a stretching sheet with slip and convective boundary conditions. J. Aerosp. Eng. 29(2): 04015037. https://doi.org/ 10.1061/(ASME)AS/1943-5525.0000529
[21] Mustafa M, Mushtaq A, Hayat T, Alsaedi A. (2015). Radiation effects in three-dimensional flow over a bi-directional exponentially stretching sheet. J. Taiwan. Inst. Chem. E. 47: 43-49. https://doi.org/ 10.1016/j.jtice.2014.10.011
[22] Butt AS, Tufail MN, Asif Ali. (2016). Three-dimensional flow of a magnetohydrodynamic Casson fluid over an unsteady stretching sheet embedded into a porous medium. J. Appl. Mech. Tech. Phys. 57(2): 283-292. https://doi.org/ 10.1134/S0021894416020115
[23] El-Aziz MA. (2007). Temperature dependent viscosity and thermal conductivity effects on combined heat and mass transfer in MHD three-dimensional flow over a stretching surface with Ohmic heating. Meccanica 42(4): 375-386. https://doi.org/ 10.1007/s11012-006-9051-5
[24] Mahanta G, Shaw S. (2015). 3D Casson fluid flow past a porous linearly stretching sheet with convective boundary condition. Alexandria Engineering Journal 54: 653-659. https://doi.org/ 10.1016/j.aej.2015.04.014
[25] Sulochana C, Ashwinkuar GP, Sandeep N. (2016). Similarity solution of 3D Casson nanofluid flow over a stretching sheet with convective boundary conditions. Journal of Nigerian Mathematical Society 35: 128-141. https://doi.org/ 10.1016/j.jnnms.2016.01.001
[26] Liao SJ. (2012). Homotopy analysis method in nonlinear differential equations. Springer & Higher Education Press, Heidelberg.
[27] Hayat T, Shehzad SA, Alsaedi A. (2012). Soret and Dufour effects on magnetohydrodynamic (MHD) flow of Casson fluid. Appl. Math. Mech. -Engl. Ed. 33(10): 1301–1312. https://doi.org/ 10.1007/s10483-012-1623-6
[28] Ibrahim SM, Kumar PV, Lorenzini G, Mabood F. (2017). Numerical study of the onset of chemical reaction and heat source on dissipative MHD stagnation point flow of Casson nanofluid over a nonlinear stretching sheet with velocity slip and convective boundary conditions. J. Eng. Thermophys 26(2): 256-271. https://doi.org/ 11.1134/S18102328170200096
[29] Kumar PV, Ibrahim SM, Lorenzini G. (2017). Impact of thermal radiation and Joule heating on MHD mixed convection flow of a Jeffrey fluid over a stretching sheet using homotopy analysis method. International Journal of Heat and Technology 35(4): 978-986. https://doi.org/ 10.18280/ijht.350434
[30] Ibrahim SM, Lorenzini G, Vijaya Kumar P, Raju CSK. (2017). Influence of chemical reaction and heat source on dissipative MHD mixed convection flow of a Casson nanofluid over a nonlinear permeable stretching sheet. Int. J. HeatMass Trans. 111: 346-355. https://doi.org/ 10.1016/j.ijheatmasstransfer.2017.03.097

NOMENCLATURE

u, v, w	velocity components in x, y, z directions, m. s^{-1}
B_0	uniform magnetic field strength, N. $m^{-1}.A^{-1}$
K^*	permeable parameter
T	Temperature, K
C	nanoparticle concentration
T_f	convective fluid temperature below the sheet, K
C_w	nanoparticle concentration at the surface of the sheet
T_∞	ambient fluid temperature, K
C_∞	ambient nanoparticle concentration
D_B	Brownian diffusion coefficient, m^2. s^{-1}
D_T	thermophoretic diffusion coefficient, m^2. s^{-1}
U_w, V_w	stretching velocities, m. s^{-1}
U_0, V_0	reference velocities, m. s^{-1}
L	reference length
M	Hartman number
Q_0	heat source coefficient
Pr	Prandtl number
Nb	Brownian motion parameter
R	radiation parameter
Nt	thermophoresis parameter
K	non-dimensional porous parameter
Q	heat source parameter
Sc	Schmidt number
Re	local Reynolds number
q_r	radiative heat flux, W. m^{-1}
q_w	wall heat flux
q_m	wall mass flux
C_{fx}, C_{fy}	skin friction coefficients along the x and y directions
Nu_x	local Nusselt number
Sh_x	Sherwood number

Greek symbols

ν_f	kinematic viscosity, $m^2. s^{-1}$
σ	electrical conductivity of the base fluid, $s. m^{-1}$
ρ_f	fluid density, $kg. m^{-3}$
α_f	thermal diffusivity, $m^2. s^{-1}$
τ	ratio between effective heat capacity of nanoparticle material and heat capacity of the fluid
β	Casson fluid parameter
h_f	convective heat transfer coefficient of the fluid
k_f	thermal conductivity of the fluid, $W. m^{-1}. k^{-1}$
σ^*	Stefan-Boltzman constant
δ	ratio parameter
B_i	Biot number
μ_f	dynamic viscosity of the fluid, $Pa.s^{-1}$
τ_{wx}, τ_{wy}	shear stresses along the x and y directions
f', g'	velocity profiles
θ	temperature profile
φ	concentration profile
k^*	mean absorption coefficient
ξ	similarity variable